Investigation of the effects of quercetin on the structure and properties of zinc-modified hydroxyapatites

Serhat Keser[1,*], Semih Kaya[2], Azeez A. Barzinjy[3,4], Bahroz Kareem Mahmood[5], Rebaz Obaid Kareem[5], Mehmet Mürşit Temüz[6], Tankut Ates[7], Suleyman Koytepe[8], Turan İnce[9], Omer Kaygili[9], Fahrettin Göktaş[9], Józef E. Sienkiewicz[10], Patryk Jasik[10], Niyazi Bulut[9,10]

[1]*Department of Chemical Technology, EOSB Vocational School, Firat University, 23119, Elazig, Turkey*

[2]*Department of Biotechnology, Institute of Science, Firat University, 23119, Elazig, Turkey*

[3]*Department of Physics, Faculty of Science, Soran University, Kurdistan Region, Iraq*

[4]*Department of Physics Education, Faculty of Education, Tishk International University, Erbil, Iraq*

[5]*Physics Department, College of Science, University of Halabja, 46018, Halabja, Iraq*

[6]*Department of Chemistry, Faculty of Science, Firat University, 23119, Elazig, Turkey*

[7]*Department of Engineering Basic Sciences, Faculty of Engineering and Natural Sciences, Malatya Turgut Özal University, Battalgazi, Malatya, Turkey*

[8]*Department of Chemistry, Faculty of Arts & Science, Inonu University, 44280, Malatya, Turkey*

[9]*Department of Physics, Faculty of Science, Firat University, 23119, Elazig, Turkey*

[10]*Faculty of Applied Physics and Mathematics, Gdańsk University of Technology, 80-952 Gdańsk, Poland*

Received 3 November 2025; received in revised form 2 February 2026; accepted 11 March 2026

Abstract

In this study, hydroxyapatite (HAp) samples, co-doped with 0.44 at.% of zinc and different amount of quercetin (Zn/Que–HAp), were synthesised using a wet-chemical method and calcined at 900 °C. XRD shows HAp as the primary phase with minor β-TCP. Compared to the Zn-doped sample without quercetin (Q1), quercetin co-doping induces clear structural changes (shifts of lattice parameters a from −0.0017 to +0.0006 nm and c from −0.0026 to −0.0005 nm), accompanied by changes in crystallinity (from −3.6% to +2.5%) and crystallite size (from −3.5 to +0.6 nm), evidencing a distinct co-doping effect. DTA/TGA reveal reduced total mass loss for the Que-containing compositions relative to the Zn-doped sample, indicating enhanced thermal stability of the co-doped lattice. SEM reveals granular morphologies with interconnected porosity, while EDX yields (Ca+Zn)/P ratios greater than 1.67, consistent with Ca-sufficient apatite and modified defect chemistry. DFT calculations resolve the site-specific effects of Zn substitution and predict a preference for perturbation at Ca2 sites. The electronic density of states retains a wide-gap, insulating character, with localised states sensitive to the dopant configuration. By correlating experiment and theory, we demonstrate that the organic-inorganic co-dopant pair offers an effective means to tune lattice metrics, phase balance, and thermal response without compromising the intrinsic insulating nature of HAp.

***Keywords**: hydroxyapatite, doping, bioceramics, thermal analysis, crystal structure*

I. Introduction

The design of advanced functional materials increasingly depends on establishing clear structure-property relationships that connect atomic-level composition with macroscopic performance. Among the most versatile systems, calcium phosphate-based ceramics, particularly hydroxyapatite (HAp, $Ca_{10}(PO_4)_6(OH)_2$), are very attractive and serve as model frameworks for exploring how chemical substitution, molecular incorporation and defect formation govern mechanical, thermal and electronic

*Corresponding author: tel: +90 4242370000
e-mail: *serhatkeser@gmail.com, skeser@firat.edu.tr*

behaviour [1–6]. Owing to its hexagonal crystal structure, HAp can accommodate a wide range of ionic and molecular dopants, enabling targeted modification of lattice strain, charge balance and crystallinity. This tuneability makes HAp not only bioceramics of biological interest, but also a prototype for multifunctional oxide-phosphate materials with potential in catalysis, coatings and dielectric or thermally resilient composites [3–6].

The calcium phosphate family (Ca:P; $Ca_3(PO_4)_2$) remains central to such design efforts because of its chemical stability, structural flexibility and compositional diversity [4–6]. Hydroxyapatite exhibits excellent mechanical integrity, chemical inertness and high thermal stability while retaining dielectric and diamagnetic characteristics - features that make it a promising material platform for coupling structural performance with functional properties [6–8]. Beyond its intrinsic stability, HAp allows for extensive ion substitution, providing a means to engineer materials with tailored lattice parameters, phase composition and defect chemistry relevant for both mechanical optimisation and biological interaction.

Zinc (Zn) represents one of the most effective modifying ions for tuning the structural and electronic characteristics of HAp. As an essential trace element stored in bone and tooth enamel, Zn regulates numerous enzymatic and mineralisation processes [9–12]. When incorporated into the HAp lattice, Zn^{2+} preferentially substitutes at Ca^{2+} sites, inducing local distortions that influence charge redistribution, crystallinity and microstructural evolution [13–16]. Zn doping has been shown to improve load-bearing capacity, resistance to corrosion and thermal stability, while preserving the insulating nature of the host lattice [17–22]. It can also modulate dielectric and mechanical behaviour through localised lattice perturbations, making Zn-doped HAp a model system for studying the interplay between composition, defect chemistry and property optimisation [23–27].

Quercetin (Que), on the other hand, is an organic modifier capable of interacting with inorganic matrices via hydrogen bonding, metal chelation, and π–π interactions [28–31]. As a naturally occurring flavonol, quercetin provides molecular functionality that can influence crystal growth dynamics, phase stabilisation and surface energy. Its redox-active and antioxidant nature allows it to affect local electronic environments, potentially modifying charge-transfer and bonding characteristics within hybrid inorganic-organic systems [28,32–36]. Quercetin incorporation has been associated with enhanced structural compactness and altered bandgap characteristics, suggesting its role as a tuneable molecular dopant that bridges inorganic rigidity with organic flexibility (Fig. 1).

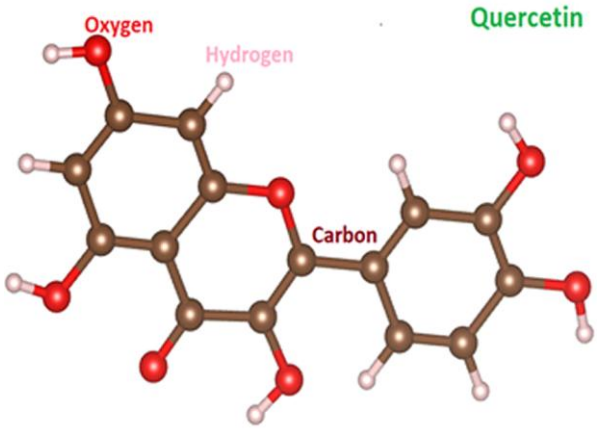

Figure 1. The geometric structure of quercetin

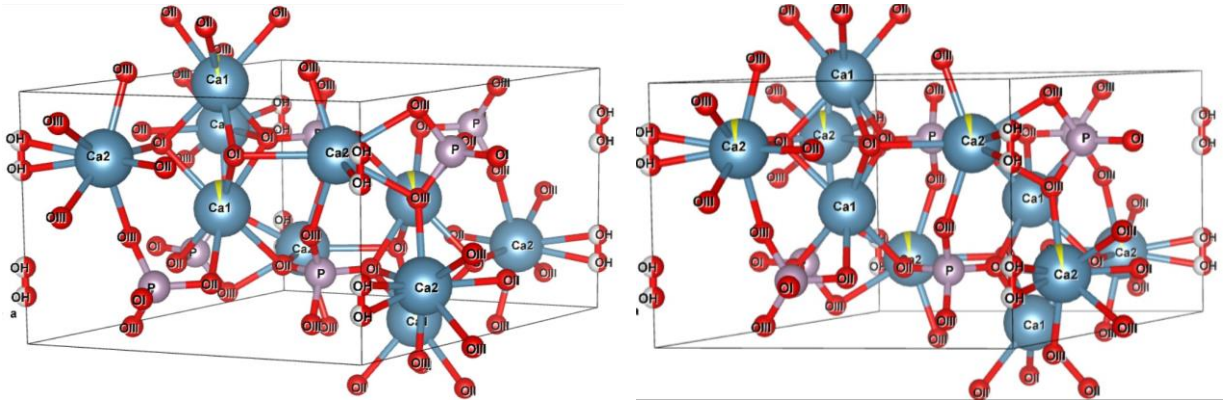

Figure 2. Crystal structure of Zn-doped hydroxyapatite (yellow parts point out the occupation of Zn for Ca sites)

Despite extensive individual investigations of Zn-doped and quercetin-modified hydroxyapatite, the combined influence of these dopants on the structural, thermal and electronic characteristics of HAp has not been previously examined. Co-doping with Zn and Que introduces both ionic and molecular perturbations, offering a route to systematically control lattice geometry, phase stability and defect-driven properties. The present study therefore focuses on the cooperative effects of inorganic (Zn) and organic (Que) dopants within the HAp framework, aiming to elucidate how dual incorporation governs the overall structure-

property relationships of the system (Fig. 2). Using a combination of controlled wet-chemical synthesis, advanced characterization (XRD, FT-IR, DTA/TGA, SEM/EDX), and density functional theory (DFT) modelling, we correlate atomic-scale substitutions with bulk responses such as crystallinity, thermal stability and electronic structure.

By integrating experimental and theoretical perspectives, this work positions Zn/Que–HAp as a model platform for multifunctional ceramics design, demonstrating how synergistic inorganic-organic co-doping strategies can be leveraged to tune lattice metrics and physical properties while retaining bioactivity. Although biomedical relevance remains an important secondary motivation, the broader aim is to establish a generalisable approach for designing structurally adaptive, thermally stable and electronically controlled ceramic systems based on compositional engineering.

II. Experimental

2.1. Synthesis

Calcium nitrate tetrahydrate ($Ca(NO_3)_2{\cdot}4H_2O$, Sigma-Aldrich), zinc acetate dihydrate ($Zn(CH_3COO)_2{\cdot}2H_2O$, Sigma-Aldrich), diammonium hydrogen phosphate ($(NH_4)_2HPO_4$, DAP, Merck) and quercetin (Sigma-Aldrich) were utilized for the synthesis of hydroxyapatite (HAp) samples. The samples were prepared via a wet chemical method, with calcium and zinc contents of 99.56 and 0.44 at.%, respectively. To investigate the effect of quercetin concentration, 0, 5, 10 and 15 ml of 0.05 M quercetin solution, dissolved in slightly basic water, were added to individual synthesis batches.

The synthesis procedure began with dissolving an appropriate amount of DAP in deionized water using a volumetric flask. In a separate container, $Ca(NO_3)_2{\cdot}4H_2O$ and $Zn(CH_3COO)_2{\cdot}2H_2O$ were dissolved in distilled water. The metal nitrate/acetate solution was then added drop-wise to the DAP solution under continuous magnetic stirring and heating to obtain the (Ca+Zn)/P molar ratio of 1.67. Subsequently, the corresponding volume of quercetin solution was added drop-wise to each batch. The reaction mixture was maintained at 80 °C for 5.5 h to form a gel-like consistency.

After gelation, the samples were dried in an oven at 200 °C for 22 h. The dried materials were then placed in porcelain crucibles and subjected to calcination in a muffle furnace at 900 °C for 4.5 h. This process yielded HAp powders with a white appearance. The final samples were labelled as Q1, Q2, Q3, and Q4, corresponding to the increasing quercetin content.

2.2. Characterisation

The synthesised hydroxyapatite (HAp) samples were characterised using a series of analytical techniques. X-ray diffraction (XRD) analysis was performed using a Rigaku RadB-Dmax II diffractometer equipped with CuKα radiation (λ = 0.15406 nm), operating at 40 kV and 40 mA. Fourier transform infrared (FT-IR) spectroscopy was conducted in the 400–4000 cm^{-1} spectral range using a PerkinElmer Spectrum One spectrometer, with samples prepared via the potassium bromide (KBr) pellet method. Surface morphology of the HAp samples was examined using a Zeiss EVO-MA10 scanning electron microscope (SEM), and the corresponding elemental composition of selected regions was analysed using an energy-dispersive X-ray spectroscopy (EDX) Bruker XFlash detector. Thermal behaviour was evaluated using differential thermal analysis (DTA) and thermogravimetric analysis (TGA), carried out on Shimadzu DTA-50 and TGA-50 instruments, respectively.

2.3. Computational details

First-principles calculations based on density functional theory (DFT) were carried out using the CASTEP code [37] implemented within the Materials Studio package. The generalised gradient approximation (GGA) was employed to describe the exchange-correlation energy using the Perdew-Burke-Ernzerhof (PBE) functional [38]. Ultrasoft pseudopotentials were used to represent the interaction between valence electrons and ionic cores [39].

The initial lattice parameters of the hexagonal hydroxyapatite (HAp) unit cell were taken as $a = b =$ 9.418 Å and $c =$ 6.884 Å as shown in Fig. 2. After the geometric optimisation, structural models for zinc substitution at two non-equivalent calcium sites (Ca1 and Ca2) were examined to assess local distortion and energetic preference. Following the structural optimisation, the unit cell parameters for the Ca1 site were refined to $a = b =$ 9.443 Å and $c =$ 6.793 Å, with a unit cell volume of 524.59 $Å^3$. For the Ca2 site, the optimized lattice parameters were $a = b =$ 9.307 Å and $c =$ 6.768 Å, with a corresponding unit cell volume of 507.73 $Å^3$. A plane-wave cut-off energy of 800 eV was initially adopted and later converged to 571.4 eV to ensure total-energy precision. The Brillouin-zone sampling was performed using a Monkhorst-Pack *k*-point mesh of 3×3×4, which provided well-converged total energies and band structures. All atomic coordinates and lattice parameters were fully relaxed until the total energy change was less than 1×10^{-5} eV/atom and the maximum force on any atom was below 0.01 eV/Å. Additionally, the calculated stress tensor components revealed minimal deviations from isotropic conditions, indicating that the structures

remained mechanically stable under the applied computational parameters.

The optimised geometries of both Ca1- and Ca2-substituted sites preserved the expected 12-fold crystallographic symmetry, confirming structural consistency within the hexagonal $P6_3/m$ space group. The calculated stress tensor components indicated isotropic mechanical behaviour under the applied computational conditions. The density of states (DOS) and band structures were computed for both substitutional configurations to evaluate dopant-induced modifications in the electronic structure. The results reveal that Zn incorporation mainly perturbs the local Ca–O coordination while retaining the wide-band-gap, insulating nature characteristic of pristine HAp.

All simulations therefore provide a consistent theoretical framework linking dopant site preference, lattice distortion, and electronic response, complementing the experimental observations of phase stability, crystallinity, and thermal resistance in the Zn/Que–HAp system.

III. Results and discussion

3.1. Electronic structure analysis

In order to investigate the ground state electronic structure of the Zn-doped hydroxyapatite systems, self-consistent field (SCF) calculations were performed using density functional theory (DFT). The simulations were carried out under non-spin polarised conditions and enforced total charge neutrality, appropriate to the closed-shell nature of the system. Strict convergence criteria were applied to ensure reliable results: the total energy per atom was converged to within 1.0×10^{-5} eV, while the eigenvalue energy convergence was set at 2.34×10^{-6} eV. The Gaussian smearing with a width of 0.1 eV was used to allow a smoother convergence and a more accurate electronic occupation near the Fermi level. The computed electronic band structure revealed characteristic electronic transitions indicative of the material's semiconducting nature, providing insights into its potential functional behaviour in biomedical and electronic applications. The convergence of the Fermi energy was tightly controlled, with a tolerance of 2.72×10^{-13} eV, ensuring high precision in determining the position of the Fermi level and the surrounding electronic states. A total of 188 energy bands were analysed, with up to 337 bands considered per *k*-point in the electronic spectroscopy analysis. This high-resolution sampling ensured adequate precision to capture the subtle features of band dispersion and the density of states (DOS), both of which are essential for a comprehensive understanding of the material's electronic properties. DOS analysis (Fig. 3) provided valuable insights into the effects of Zn substitution on the electronic structure of hydroxyapatite. In particular, subtle modifications were observed near the conduction band minimum (CBM) and the valence band maximum (VBM), depending on the substitution site (Ca1 or Ca2). These modifications, while maintaining the wide band gap and insulating character of the parent HAp structure, indicate localised electronic perturbations that may impact charge transport and surface reactivity. Such alterations have the potential to enhance the material's interactions with biological systems, particularly in contexts where electronic properties are implicated in bioactivity, such as protein adsorption, cellular signalling or redox-mediated antimicrobial mechanisms.

Overall, the self-consistent field (SCF) based electronic structure analysis confirms both the structural integrity and electronic stability of Zn-doped hydroxyapatite (HAp). These findings provide a robust theoretical foundation for the continued exploration of Zn-doped HAp as a multifunctional platform in biomedical applications, particularly in areas such as bone tissue engineering, implant surface modification, and antimicrobial therapies, where material stability and electronic characteristics play a critical role in performance and biocompatibility.

Structural optimisation and forces

Atomic relaxation was carried out to obtain the equilibrium geometry, minimising the total forces acting on each ion. The force tolerance was maintained at 0.01 eV/Å, ensuring high accuracy in the optimised geometry. The maximum calculated force exerted on any atom remained within acceptable convergence thresholds, thereby confirming the structural stability of the system. Furthermore, the atomic forces acting on oxygen, phosphorus, calcium and zinc atoms exhibited a symmetric distribution, indicating minimal deviations from the ideal lattice symmetry and further supporting the equilibrium configuration of the doped structure. The system contained two distinct calcium sites, Ca1 and Ca2, each exhibiting different substitutional behaviour upon Zn incorporation. For the Ca1 site, Zn substitution was found at a level of approximately 1.1%, corresponding to four Zn atoms replacing Ca atoms in a 48-ion unit cell. The forces acting on Zn-substituted Ca1 sites exhibited minimal deviations from the undisturbed lattice, with an average force magnitude of –0.00823 eV/Å, indicating a negligible perturbation to the local atomic environment.

Analysis of the stress tensor components further revealed an almost imperceptible impact on the mechanical stability at these substitutional sites. In the case of Ca2 sites, approximately 12% Zn incorporation was achieved, corresponding to the replacement of six calcium atoms by zinc within a 50-atom unit cell.

Although the Zn substitution at Ca2 sites resulted in slightly higher force deviations, particularly along the *z*-direction with an average force of –0.00874 eV/Å, the structural integrity of the lattice was preserved. This was corroborated by the symmetrised stress tensor components, which indicated that the doped structure retained its mechanical and crystallographic stability.

Spectral properties

Electronic spectroscopy calculations were carried out to further investigate the effects of Zn substitution on the electronic structure of hydroxyapatite (HAp). The calculations focused on the analysis of the density of states (DOS) and electronic band dispersion, both of which are essential for elucidating the electronic behaviour of doped materials. To ensure spectral convergence and computational accuracy, the maximum number of self-consistent iterations was set to 999, facilitating the generation of stable and reliable band structure and DOS profiles. The results demonstrated the preservation of the overall band structure, with distinct identification of key electronic transitions in the vicinity of the Fermi level, thereby supporting the electronic stability of the doped system. The DOS profiles in Fig. 3 reveal subtle site-dependent variations in the electronic structure upon Zn substitution. For the Ca1 site, the DOS remains nearly identical to that of pristine HAp, suggesting minimal perturbation to the electronic framework. In contrast, substitution at the Ca2 site introduces shallow localised states near the conduction band minimum, indicating slight charge redistribution around Zn–O coordination environments. This difference reflects the structural asymmetry between the Ca1 and Ca2 environments and highlights the sensitivity of local electronic states to the dopant site selection. Despite these perturbations, both configurations maintain the wide band gap (~5 eV), confirming that Zn incorporation does not compromise the insulating character crucial for biomedical and dielectric applications where insulating surfaces reduce the risk of electrochemical interference and improve biocompatibility [17,22]. The observed variations in the density of states (DOS) and band structure between the Ca1 and Ca2 substitution sites highlight the site-specific electronic effects induced by Zn doping. While substitution at Ca1 is electronically benign, Ca2 doping leads to the localised changes that could influence charge redistribution, ion exchange potential and surface reactivity. These subtle electronic modifications have the potential to enhance the material's interactions with biomolecules, thereby improving its functional performance in biomedical applications such as implant coatings, drug delivery systems, and bone regeneration scaffolds [17,22].

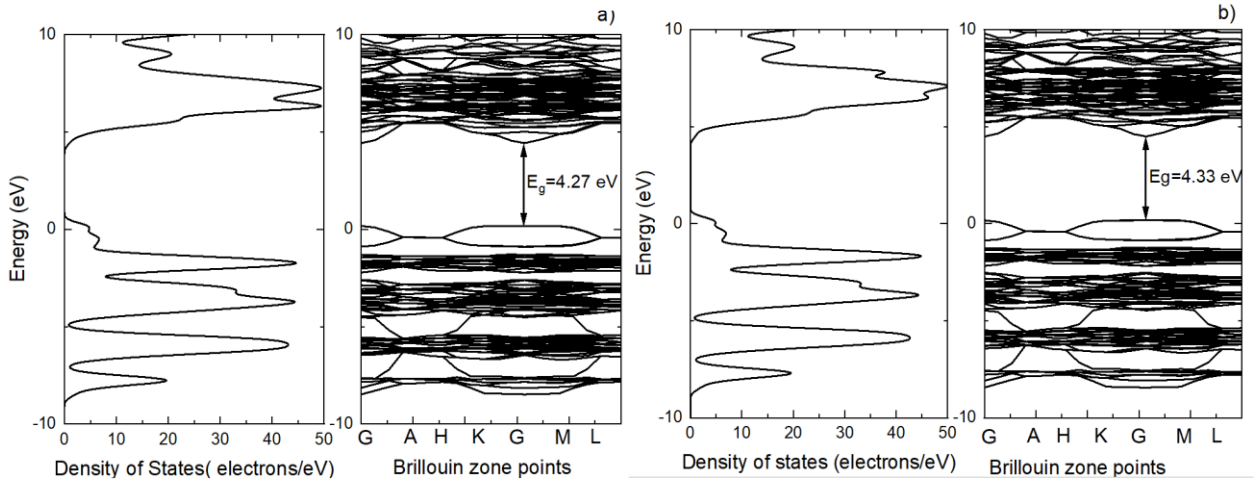

Figure 3. Total electronic density of states (DOS) and corresponding band gap structures for Zn-doped hydroxyapatite models: a) Zn substituted at the Ca1 site and b) Zn substituted at the Ca2 site. Zn incorporation at distinct Ca sites induces localized modifications near the conduction and valence band edges, while the wide-gap insulating nature of hydroxyapatite is retained

In particular, the potential for Zn to modulate the charge transport properties of HAp, without compromising its insulating matrix, may support more effective biological communication at the material-tissue interface. The incorporation of Zn at Ca2 site could enhance bioactivity by promoting cell adhesion and stimulating enzymatic processes associated with osteogenesis and antibacterial defence [17]. Thus, the results presented in Fig. 3 not only confirm the structural and electronic stability of Zn-doped HAp, but also highlight the importance of dopant site selection in tailoring material functionality for biomedical applications.

Dual-doped HAp materials are commonly engineered using ion-ion or ion-anion combinations to introduce synergistic functionalities. Representative examples include Sr/Zn co-doped systems targeting concurrent osteogenic performance [40], Sr/Mg co-doped HAp for structural/mechanical tuning and Cu/Zn co-doped HAp for multifunctional biological

and physicochemical responses. Ion-anion strategies such as Zn/F and Zn/Na [41] have also been reported to modulate surface chemistry and functional behaviour. Distinct from these mainly inorganic co-doping routes, the present work adopts an organic–inorganic co-doping concept: Zn is incorporated at trace level in the apatite lattice while quercetin is introduced as a molecular modifier (Zn/Que–HAp), enabling coupled control of lattice/defect chemistry and thermal response, supported by site-specific DFT analysis of Zn substitution.

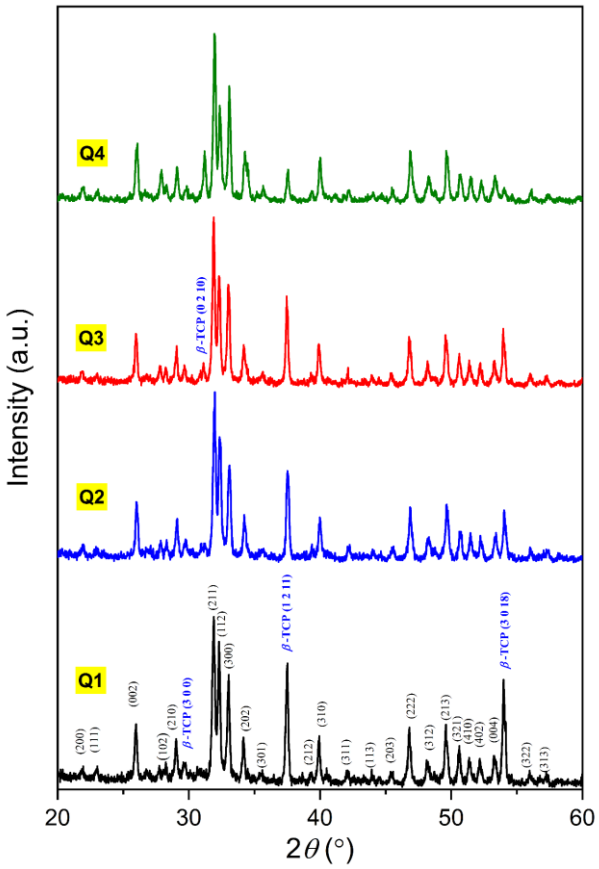

Figure 4. XRD patterns of the synthesised Zn/Que-HAp samples

3.2. Experimental results

XRD results

XRD patterns of the synthesised hydroxyapatite (HAp) samples are presented in Fig. 4. Analysis of the diffraction data confirms that hydroxyapatite (HAp), corresponding to JCPDS card No. 09-0432, is the predominant crystalline phase in all samples. A secondary phase, identified as *β*-tricalcium phosphate (*β*-TCP), is also present, in accordance with JCPDS card no. 09-0169. Detailed examination of the diffraction profiles reveals discernible modifications in phase composition and peak intensities attributable to the incorporation of quercetin and Zn dopants. These changes suggest that both additives influence the crystallisation behaviour and phase stability of the material, potentially altering its structural and functional properties.

The average crystallite size (D) for all samples was determined using the Scherrer equation, providing an estimate of the average crystallite dimensions based on the broadening of X-ray diffraction peaks [42]:

$$D = \frac{0.9 \cdot \lambda}{\beta \cdot \cos\theta} \quad (1)$$

where β represents the full width at half maximum, λ represents the X-ray wavelength and θ represents the Bragg angle. The average crystallite size for the samples was calculated separately as D_{002} and D_{300} for the (002) and (300) planes, respectively, and the obtained values are shown in Table 1.

The lattice parameters (a and c) and unit cell volume (V) were calculated using the appropriate equations, as outlined below [42].

$$\frac{1}{d^2} = \frac{4}{3}\left(\frac{h^2 + hk + k^2}{a^2}\right) + \frac{l^2}{c^2} \quad (2)$$

$$V = 0.866 \cdot a^2 c \quad (3)$$

where the symbols h, k and l denote the Miller indices, which characterise the crystallographic planes in the material's lattice structure. The crystallisation percentages (X_C) of the samples were determined using the equation reported by Landi *et al*. [43]:

$$X_C = \left(1 - \frac{V_{112/300}}{I_{300}}\right) \times 100 \quad (4)$$

In this equation, $V_{112/300}$ represents the intensity of the trough between the (112) and (300) reflections, and I_{300} represents the intensity of the reflection belonging to the (300) plane [44]. All parameters derived from the XRD data analysis, as previously discussed, are summarised in Table 1.

Upon examination of the results presented in Table 1 it is evident that all calculated parameters are notably influenced by the incorporation of both quercetin and Zn additives. Specifically, the lattice parameters a and c of the synthesised HAp samples exhibit significant alterations, while the crystallisation ranges between 80.0% and 86.1%.

Keser and Efe [45] demonstrated that chitosan significantly influenced the crystallite size, lattice parameters, unit cell volume and crystallinity of chitosan-doped Zn-based hydroxyapatite (HAp) samples. Similarly, Habib *et al*. [46] reported that the crystal structure parameters of HAp samples doped with 5 at.% Zn were a = 9.417 Å, c = 6.884 Å and unit cell volume of 528.69 Å^3, with crystallite size of 59.69 nm and HAp phase purity of 100%,. Mardziah *et al*. [22] found that HAp samples doped with 5, 10 and 15 at.% Zn and calcined at 700 °C contained HAp and *β*-

TCP phases with crystallinity in the range of 43–54% and the average crystallite size of the HAp phase in the range of 30.3–32.8 nm. They also found that the crystal structure parameters were in the range of a = 9.389–9.422 Å and c = 6.845–6.852 Å. In another study, Aqib *et al*. [47] determined that the crystal parameters of the brushite samples were affected by the Zn^{2+} doping. Sun *et al*. [48] showed that the crystal structure parameters of HAp samples doped with 1, 5 and 10 at.% Zn were in the range of a = 9.392–9.404 Å, c = 6.868–6.879 Å and the volume of unit cell values were 524.7–526.5 $Å^3$. Bulina *et al*. [49] and Chaikina *et al*. [50] found that the lattice parameters of Zn-doped HAp samples synthesised by low-temperature mechanochemical method were affected by Zn doping. Previous studies have reported that the incorporation of quercetin significantly influences the bandgap, crystallite size, crystallinity, lattice parameters and morphology of both Au-based [51] and Ag-based hydroxyapatite (HAp) samples [52].

Table 1. Parameters obtained as a result of detailed XRD analysis of the synthesised samples

Samples	a [nm]	c [nm]	V [nm^3]	X_C [%]	D [nm]
Q1	0.9389	0.6859	0.5236	83.6	41.17
Q2	0.9373	0.6843	0.5206	80.0	37.67
Q3	0.9395	0.6854	0.5239	85.6	40.10
Q4	0.9372	0.6833	0.5197	86.1	41.80

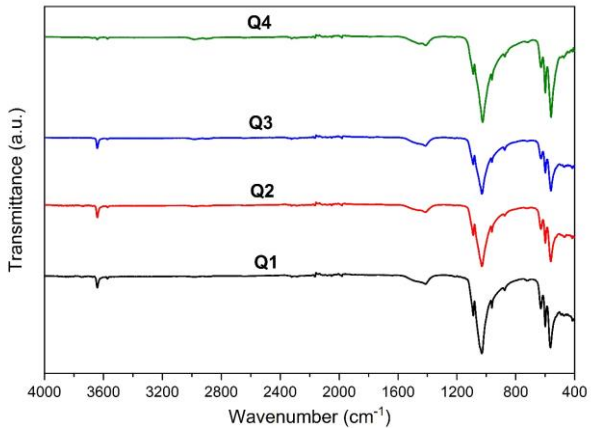

Figure 5. FT-IR spectra of Zn/Que–HAp samples with different amounts of quercetin

FT-IR Analyses

FT-IR spectra of the Zn-doped HAp samples containing different amounts of quercetin (0, 5, 10 and 15 ml) are presented in Fig. 5. The bands related to the phosphate (PO_4^{3-}) group were detected at 471, 566, 600, 962, 1031 and 1089 cm^{-1} for all samples (Q1, Q2, Q3 and Q4) [44,53-55]. Similarly, Habib *et al*. [46] showed that HAp samples doped with 5 at.% Zn had peaks at wavenumbers of 1085, 1026, 955, 595, 567 and 472 cm^{-1} as a result of FT-IR analysis. The characteristic vibrational bands corresponding to the OH^- (hydroxyl) group were observed at 630 and 3642 cm^{-1} in all samples [56,57]. Aqib *et al*. [47] showed that the brushite samples doped with Zn^{2+} exibited 1652 cm^{-1} H_2O bending and 3540 cm^{-1} O–H stretching peaks. Mardziah *et al*. [22] showed that the HAp samples doped with 5, 10 and 15 at.% Zn calcined at 700 °C carried OH^- functional groups in liberation mode at 632 cm^{-1} and stretching mode at 3571 cm^{-1} peaks. Finally, the characteristic absorption bands corresponding to the carbonate (CO_3^{2-}) group were observed at 876 cm^{-1}, 1414 cm^{-1} and 1463 cm^{-1} in all samples [57]. In a similar study, Sun *et al*. [48] identified carbonate (CO_3^{2-}) group peaks in HAp samples doped with 1, 5, and 10 at.% Zn. The FT-IR spectra further confirm that all synthesised samples (Q1, Q2, Q3 and Q4) exhibit the characteristic functional groups of HAp, indicating the formation of stable products.

Quercetin is not expected to substitute into the HAp bulk lattice as an intact molecule, rather, it most plausibly interacts with HAp through surface/defect binding. Two main modes are likely: i) inner-sphere coordination where quercetin acts as an O-donor ligand (carbonyl/phenolic oxygens) binding to exposed Ca sites (or Zn when substituted at Ca sites), and ii) outer-sphere hydrogen bonding with phosphate oxygens and surface OH^- groups. Our DFT results showing a stronger perturbation/preference associated with the Ca2 environment suggest that quercetin binding should be favoured at Ca2-like exposed sites and in Zn-affected Ca neighbourhoods, providing a mechanistic rationale for the observed property changes upon quercetin incorporation.

Thermal analysis

Figure 6 presents DTA results for the Zn-based samples containing varying amounts of quercetin. An endothermic peak observed around 400 °C is likely attributed to the release of water molecules trapped within the crystal structure [58,59]. Additionally, an exothermic peak observed near 650 °C can be associated with the dehydroxylation process occurring within the apatite structure [60]. Figure 7 shows TGA curves of the synthesised samples, highlighting their thermal stability and mass loss behaviour over the temperature range. All samples exhibit a similar thermal degradation pattern, characterised by a progressive mass loss as the temperature increases.

This behaviour is typical of hydroxyapatite-based biomaterials and is primarily attributed to the evaporation of physically adsorbed water, the decomposition of residual organic matter and the structural dehydroxylation processes. The total mass loss values observed were 4.18%, 2.56%, 3.79% and 2.45% for the Q1, Q2, Q3 and Q4 samples, respectively. Notably, the quercetin containing samples (Q2, Q3 and Q4) showed lower total mass loss compared to the Zn-doped sample (Q1), indicating improved thermal stability upon quercetin incorporation. This improved stability may be due to the interaction between quercetin molecules and the HAp matrix, possibly forming hydrogen bonds or chelating with calcium or zinc ions, which could hinder thermal decomposition and limit moisture desorption. The minor variation in mass loss observed among the quercetin-containing samples can be attributed to the amount of quercetin incorporated during synthesis, which influences the organic content and the binding strength within the matrix. Furthermore, the presence of Zn may enhance the structural compactness and thermal stability of the material by reinforcing the HAp lattice and stabilising the crystal structure at elevated temperatures. In comparison, Mardziah *et al*. [22] reported higher mass losses of 5.4%, 6.2% and 6.4% for Zn-doped HAp samples containing 5, 10 and 15 at.% Zn, respectively, when subjected to thermal analysis from 30 to 700 °C. These higher values suggest that co-doping with both Zn and quercetin, as performed in the present study, may contribute to a more thermally stable composite than Zn-only doped counterparts. This reinforces the role of quercetin not only as a bioactive compound but also as a thermal stabiliser within the HAp matrix.

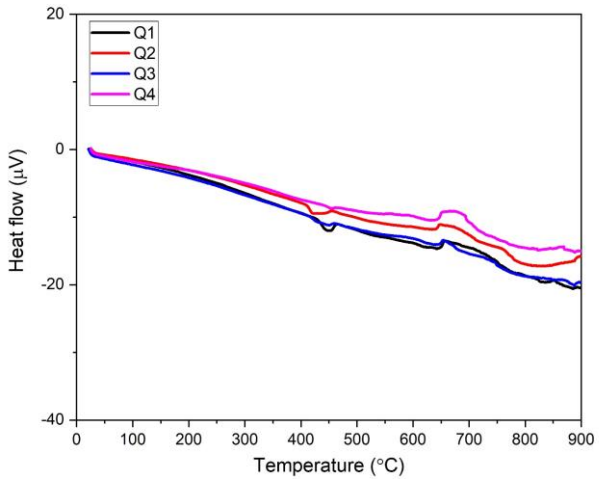

Figure 6. DTA thermograms of the as-produced samples

The observed thermal behaviour provides additional evidence supporting the suitability of the Zn/Que-HAp materials for biomedical applications, particularly in contexts where thermal stability is crucial. This includes scenarios such as sterilisation processes and high-temperature treatments, where maintaining structural integrity and functional properties under elevated temperatures is a critical consideration. The enhanced thermal resistance exhibited by these materials suggests their potential for use in environments that demand high levels of durability and stability, making them promising candidates for a range of biomedical applications, including implantable devices, drug delivery systems, and tissue engineering scaffolds.

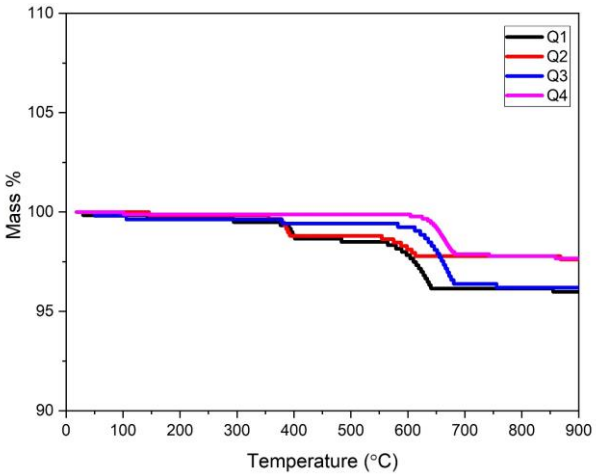

Figure 7. TGA thermograms of the as-produced HAp samples

SEM and EDX analyses

The morphological and elemental characteristics of the synthesised samples were analysed using SEM and EDX spectroscopy, with the results presented in Fig. 8. The SEM images revealed that all samples exhibited a granular morphology, characterised by uniformly distributed small grains and interconnected porosity. This microstructural configuration is highly beneficial for biomedical applications, particularly in bone tissue engineering, as it facilitates cell attachment, proliferation and nutrient diffusion through the porous network. Additionally, the presence of porosity supports the integration of the biomaterial with natural bone tissue, thereby enhancing osteointegration and promoting effective tissue regeneration. Quantitative elemental analysis using EDX gave (Ca+Zn)/P molar ratios of 3.306, 1.966, 3.044 and 2.548 for the Q1, Q2, Q3 and Q4 samples, respectively. These ratios are significantly different from the theoretical stoichiometric ratio of 1.67 characteristic of pure hydroxyapatite. The elevated values observed in all samples suggest the formation of Ca-sufficient hydroxyapatite (CDHAp), a variant recognised for its enhanced bioresorbability and improved biological performance. This deviation indicates that the incorporation of Zn and quercetin influences the overall Ca/P ratio, potentially through

the substitution of Ca ions or interaction with phosphate groups. Such modifications are likely to alter the crystal lattice structure and surface chemistry of the material. These structural changes may significantly contribute to the improved biological and physicochemical properties of the doped HAp materials, including enhanced solubility, controlled ion release behaviour and superior antibacterial performance [43,44].

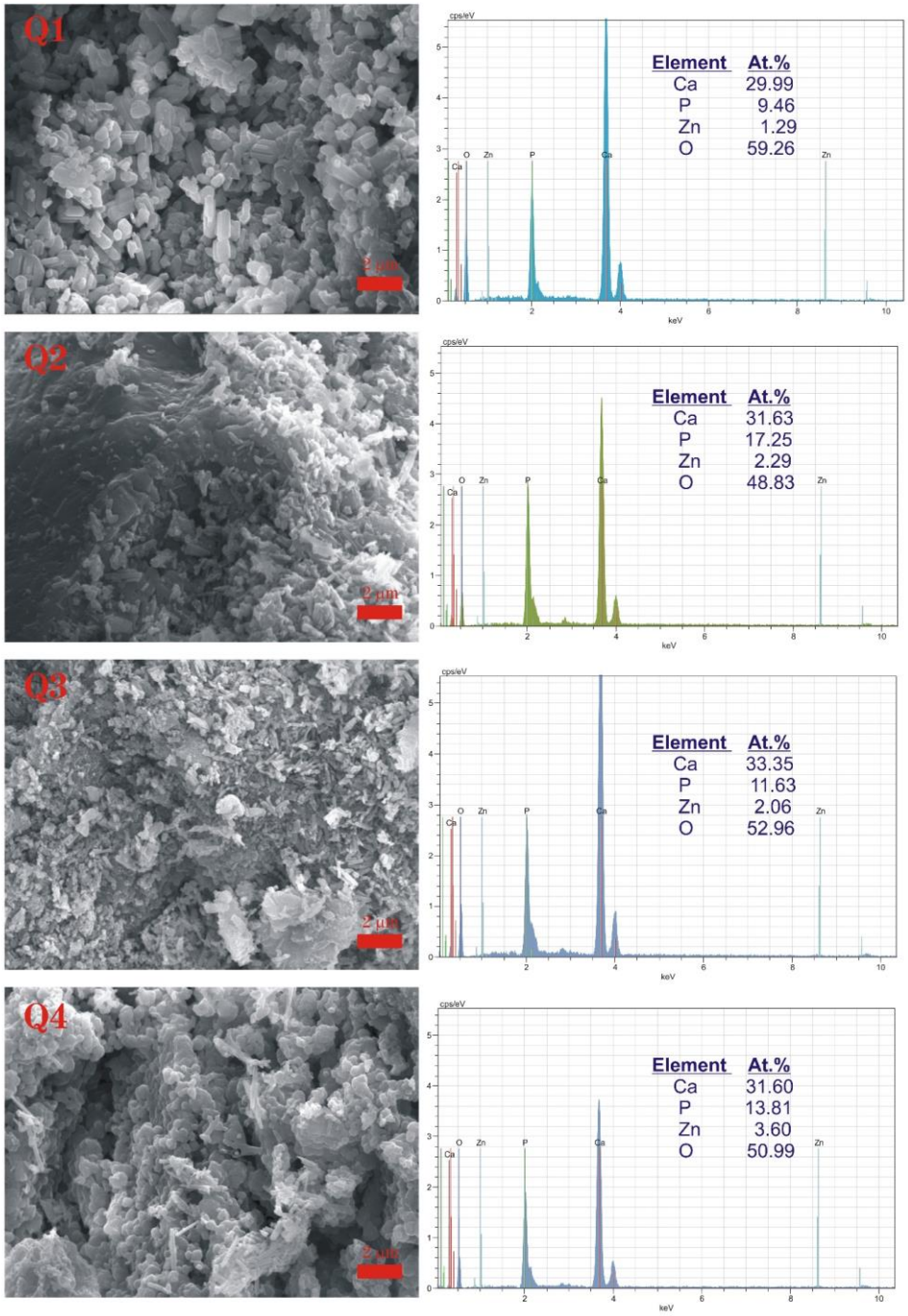

Figure 8. Morphological investigation of the samples using SEM and EDX analysis

Importantly, while numerous studies have previously investigated the individual doping of hydroxyapatite (HAp) with either Zn or quercetin, the current study represents the first known synthesis of co-doped Zn/Que-HAp structures. This novel combination introduces synergistic effects, with Zn contributing to enhanced osteogenic and antibacterial activity, while quercetin imparts additional benefits, including antioxidant, anti-inflammatory and further antibacterial properties. The successful co-doping of HAp with both Zn and quercetin, while preserving the material's purity and structural integrity, represents a significant advancement in the development of multifunctional biomaterials. These findings highlight

the potential of Zn/Que-HAp composites for use in a variety of advanced biomedical applications, such as bone grafting, implant coatings and other regenerative medicine strategies. The unique combination of therapeutic properties offered by this co-doping strategy underscores its promising role in enhancing the effectiveness of biomaterials used for tissue regeneration and disease prevention.

IV. Conclusions

This study represents the first demonstration of hydroxyapatite co-doped with metal ion (Zn^{2+}) and organic flavonoid (quercetin), revealing unique cooperative lattice-electronic interactions arising from the synergistic interplay between molecular and ionic dopants and integrating compositional engineering with experimental and theoretical analysis. Co-doping systematically modifies lattice parameters, crystallinity and defect chemistry while preserving the intrinsic insulating character of HAp. The complementary roles of Zn and quercetin, ionic substitution and molecular interaction, lead to enhanced structural stability, improved thermal resistance and finely tuneable microstructure. Density functional theory (DFT) calculations further reveal site-specific effects of Zn substitution, linking local coordination environments to the changes in electronic density of states. The results highlight that controlled co-doping offers a robust route to tailor mechanical, electronic and thermal properties of calcium-phosphate ceramics without compromising their phase integrity. Such tuneability makes Zn/Que–HAp an archetype for designing multifunctional materials that couple inorganic rigidity with organic flexibility, suitable for applications ranging from dielectric coatings and catalytically active surfaces to bioactive interfaces. The biomedical relevance, manifested through maintained biocompatibility and potential osteogenic activity, serves as a secondary but meaningful outcome of this broader materials design strategy. Overall, this work demonstrates how integrated experiment-theory approaches can guide the rational development of multifunctional oxide–phosphate systems with both structural and functional adaptability. As a future work, biological properties and biocompatibility of the samples can be investigated in detail.

Acknowledgement: This work was supported by the Management Unit of Scientific Research Projects of Firat University (FUBAP) (Project Numbers: MMY.21.05, ADEP.24.01, ADEP.24.09 and ADEP.25.06). NB gratefully acknowledge the support of the Nobelium Joining Gdańsk Tech Research Community, number: DEC-1/12025/IDUB/I.1a/No: 038122.

References

1. S. Medici, M. Peana, G. Crisponi, V.M. Nurchi, J.I. Lachowicz, M. Remelli, M.A. Zoroddu, “Silver coordination compounds: A new horizon in medicine”, *Coordinat. Chem. Rev.*, **327** (2016) 349–359.
2. K.D. Mjos, C. Orvig, “Metallodrugs in medicinal inorganic chemistry”, *Chem. Rev.*, **114** (2014) 4540–4563.
3. S. Bose, G. Fielding, S. Tarafder, A. Bandyopadhyay, “Understanding of dopant-induced osteogenesis and angiogenesis in calcium phosphate ceramics”, *Trends Biotechnol.*, **31** (2013) 594–605.
4. B. Yilmaz, A.Z. Alshemary, Z. Evis, “Co-doped hydroxyapatites as potential materials for biomedical applications”, *Microchem. J.*, **144** (2019) 443–453.
5. S.V. Dorozhkin, “Calcium orthophosphates in nature, biology and medicine”, *Materials*, **2** (2009) 399–498.
6. R.O. Kareem, O. Kaygili, T. Ates, N. Bulut, S. Koytepe, A. Kuruçay, F. Ercan, I. Ercan, “Experimental and theoretical characterization of Bi-based hydroxyapatites doped with Ce”, *Ceram. Int.*, **48** (2022) 33440–33454.
7. R.O. Kareem, N. Bulut, O. Kaygili, “Hydroxyapatite biomaterials: a comprehensive review of their properties, structures, medical applications, and fabrication methods”, *J. Chem. Rev.*, **6** (2024) 1–26.
8. N. Bulut, O. Kaygili, A.H. Hssain, S.V. Dorozhkin, B. Abdelghani, C. Orek, H. Kebiroglu, T. Ates, R.O. Kareem, “Mg-dopant effects on band structures of Zn-based hydroxyapatites: A theoretical study”, *Iran. J. Sci.*, **47** (2023) 1843–1859.
9. D. Lahiri, S. Ghosh, A. Agarwal, “Carbon nanotube reinforced hydroxyapatite composite for orthopedic application: a review”, *Mat. Sci. Eng. C*, **32** (2012) 1727–1758.
10. E.A. Ofudje, A.I. Adeogun, M.A. Idowu, S.O. Kareem, “Synthesis and characterization of Zn-doped hydroxyapatite: scaffold application, antibacterial and bioactivity studies”, *Heliyon*, **5** (2019) e01716.
11. M. Yamaguchi, R. Yamaguchi, “Action of zinc on bone metabolism in rats: increases in alkaline phosphatase activity and DNA content”, *Biochem. Pharmacol.*, **35** (1986) 773–777.
12. M. Yamaguchi, H. Oishi, Y. Suketa, “Stimulatory effect of zinc on bone-formation in tissue-culture”, *Biochem. Pharmacol.*, **36** (1987) 4007–4012.
13. X. Wang, A. Ito, Y. Sogo, X. Li, A. Oyane, “Zinc-containing apatite layers on external fixation rods promoting cell activity”, *Acta Biomater.*, **6** (2010) 962–968.
14. E. Jallot, J.M. Nedelec, A.S. Grimault, E. Chassot, A. Grandjean-Laqueriere, P. Laquerriere, D. Laurent-Maquin, “STEM and EDXS characterisation of physico-chemical reactions at the periphery of sol-gel derived Zn-substituted hydroxyapatites during interactions with biological fluids”, *Colloids Surf. B*, **42** (2005) 205–210.
15. F. Velard, D. Laurent-Maquin, J. Braux, C. Guillaume, S. Bouthors, E. Jallot, J.M. Nedelec, A. Belaaouaj, P. Laquerriere, “The effect of zinc on hydroxyapatite-mediated activation of human polymorphonuclear neutrophils and bone implant-associated acute inflammation”, *Biomaterials*, **31** (2010) 2001–2009.

16. K. Matsunaga, H. Murata, T. Mizoguchi, A. Nakahira, "Mechanism of incorporation of zinc into hydroxyapatite", *Acta Biomater.*, **6** (2010) 2289–2293.
17. V. Saxena, A. Hasan, L.M. Pandey, "Effect of Zn/ZnO integration with hydroxyapatite: a review", *Mater. Technol.*, **33** (2018) 79–92.
18. S. Take, M. Kato, T. Asami, Y. Aihara, S. Izawa, T. Atsumi, "Evaluation of Zn doped hydroxyapatite plasma spray biocompatible coatings on metallic substrates", *ECS Trans.*, **75** (2017) 149–155.
19. R. Kaur, A. Hasan, N. Iqbal, S. Alam, M.K. Saini, S.K. Raza, "Synthesis and surface engineering of magnetic nanoparticles for environmental cleanup and pesticide residue analysis: a review", *J. Sep. Sci.*, **37** (2014) 1805–1825.
20. I. Manjubala, P. Ganesan, U. Narendrakumar, B. Madhan, "Fabrication of BCP-cellulose composite scaffolds for bone regeneration", *Orthop Procs.*, **99B** (2017) 45.
21. A.Z. Alshemary, A.E. Pazarceviren, A. Tezcaner, Z. Evis, "Fe^{3+}/SeO_4^{2-} dual doped nano hydroxyapatite: a novel material for biomedical applications", J. *Biomed. Mater. Res. Part B Appl Biomater.*, **106** (2018) 340–352.
22. C.M. Mardziah, S. Ramesh, M.F. Abdul Wahid, H. Chandran, A. Sidhu, S. Krishnasamy, J. Purbolaksono, "Effect of zinc ions on the structural characteristics of hydroxyapatite bioceramics", *Ceram. Int.*, **46** (2020) 13945–13952.
23. P. Bhattacharjee, H. Begam, A. Chanda, S.K. Nandi, "Animal trial on zinc doped hydroxyapatite: A case study", *J. Asian Ceram. Soc.*, **2** (2014) 44–51.
24. A. Bigi, E. Foresti, M. Gandolfi, M. Gazzano, N. Roveri, "Inhibiting effect of zinc on hydroxylapatite crystallization", *J. Inorg. Biochem.*, **58** (1995) 49–58.
25. T.J. Webster, C. Ergun, R.H. Doremus, R. Bizios, "Hydroxylapatite with substituted magnesium, zinc, cadmium, and yttrium. II. Mechanisms of osteoblast adhesion", *J. Biomed. Mater. Res.*, **59** (2002) 312–317.
26. A. Bandyopadhyay, E.A. Withey, J. Moore, S. Bose, "Influence of ZnO doping in calcium phosphate ceramics", *Mater. Sci. Eng. C*, **27** (2007) 14–17.
27. O. Kaygili, C. Tatar, "The investigation of some physical properties and microstructure of Zn-doped hydroxyapatite bioceramics prepared by sol–gel method", *J. Sol-Gel Sci. Technol.*, **61** (2012) 296–309.
28. M. Materska, "Quercetin and its derivatives: chemical structure and bioactivity-a review", *Pol. J. Food Nutr. Sci.*, **58** (2008) 407–413.
29. A. Samadi, M. Pourmadadi, F. Yazdian, H. Rashedi, M. Navaei-Nigjeh, "Ameliorating quercetin constraints in cancer therapy with pH-responsive agarose-polyvinylpyrrolidone-hydroxyapatite nanocomposite encapsulated in double nanoemulsion", *Int. J. Biol. Macromol.*, **182** (2021) 11–25.
30. X. Yi, F. Bao, S. Fu, Y. Yang, Y. Xu, "Preparation of mesoporous silica/hydroxyapatite loaded quercetin nanoparticles and research on its antibacterial properties", *Med. Eng. Phys.*, **26** (2024) 104160.
31. X. Liu, K. Lin, R. Qian, L. Chen, S. Zhuo, J. Chang, "Growth of highly oriented hydroxyapatite arrays tuned by quercetin", *Chemistry*, **18** (2012) 5519–5523.
32. J. Yang, L. Zhang, Q. Ding, S. Zhang, S. Sun, W. Liu, J. Liu, X. Han, C. Ding, "Flavonoid-loaded biomaterials in bone defect repair", *Molecules*, **28** (2023) 6888.
33. J.E. Song, N. Tripathy, D.H. Lee, J.H. Park, G. Khang, "Quercetin inlaid silk fibroin/hydroxyapatite scaffold promotes enhanced osteogenesis", *ACS Appl. Mater. Interfaces*, **10** (2018) 32955–32964.
34. J. Kim, Y.J. Choi, H. Park, H.S. Yun, "Fabrication of multifunctional alginate microspheres containing hydroxyapatite powder for simultaneous cell and drug delivery", *Front. Bioeng. Biotechnol.*, **10** (2022) 827626.
35. X. Yang, Q. Lai, J. Guo, X. Yang, W. Zhu, S. Zhou, M. Liu, X. Zhang, B. Zhang, Y. Wei, "Facile fabrication of phosphazene-quercetin-alendronate composites as pH-responsive bone-targeted nanomedicine for osteoporosis treatment", *Mater. Des.*, **241** (2024) 112968.
36. Y. Zhou, Y. Wu, W. Ma, X. Jiang, A. Takemra, M. Uemura, L. Xia, K. Lin, Y. Xu, "The effect of quercetin delivery system on osteogenesis and angiogenesis under osteoporotic conditions", *J. Mater. Chem. B*, **5** (2017) 612–625.
37. S.J. Clark, M.D. Segall, C.J. Pickard, P.J. Hasnip, M.I.J. Probert, K. Refson, M.C. Payne, "First principles methods using CASTEP", *Z. Kristallogr. Cryst. Mater.*, **220** (2005) 567–570.
38. J.P. Perdew, K. Burke, M. Ernzerhof, "Generalized gradient approximation made simple", *Phys. Rev. Lett.*, **77** (1996) 3865–3868.
39. D. Vanderbilt, "Soft self-consistent pseudopotentials in a generalized eigenvalue formalism", *Phys. Rev. B Condens. Matter*, **41** (1990) 7892–7895.
40. J. Yao, C. Huang, J. Yao, J. Hui, S. Shen, X. Zheng, L. Shen, D. Fan, "A moldable hydrogel based on sericin and Zn^{2+}/F^- dual-doped hydroxyapatite promotes skull defect repair through the synergistic effects of immunoregulation, enhanced angiogenesis and osteogenesis", *Chem. Eng. J.*, **491** (2024) 151789.
41. H. Samadi, P. Samadi Pakchin, M. Mohammadpourfard, K. Adibkia, "Zn/Na co-doped hydroxyapatites: Synthesis, antibacterial, and bioactivity studies", *Mat. Chem. Phys.*, **341** (2025) 130833.
42. B.D. Cullity, "Elements of X-ray Diffraction", 2nd Edition, Addison–Wesley Publishing Company, Massachusetts, 1987.
43. E. Landi, A. Tampieri, G. Celotti, S. Sprio, "Densification behaviour and mechanisms of synthetic hydroxyapatites", *J. Eur. Ceram. Soc.*, **20** (2000) 2377–2387.
44. G. Mabilleau, R. Filmon, P.K. Petrov, M.F. Baslé, A. Sabokbar, D. Chappard, "Cobalt, chromium and nickel affect hydroxyapatite crystal growth *in vitro*", *Acta Biomater.*, **6** (2010) 1555–1560.
45. S. Keser, H. Efe, "Investigation of *in vitro* bioactivities of Zn-based hydroxyapatites samples doped with chitosan", *J. Aust. Ceram. Soc.*, **57** (2021) 117–124.
46. L. Habib, S.A. Disha, S. Hossain, N. Uddin, S. Ahmed, "Enhancement of antimicrobial properties by metals doping in nano-crystalline hydroxyapatite for efficient biomedical applications", *Heliyon*, **10** (2024) e23845.
47. M. Aqib, M. Alomar, A. Anwar, K. Naseem, A. Javaid, A. Intisar, S. Khan, H. Ajaz, I.H. Khan, "Synthesis, characterization and antimicrobial analysis of metal-doped (Zn^{2+} and Ag^+) brushite powder for bone regeneration", *Mater. Chem. Phys.*, **320** (2024) 129460.
48. G. Sun, J. Ma, S. Zhang, "Electrophoretic deposition of zinc-substituted hydroxyapatite coatings", *Mater. Sci. Eng. C.*, **39** (2014) 67–72.

49. N.V. Bulina, M.V. Chaikina, O.B. Vinokurova, I.Y. Prosanov, N.Z. Lyakhov, "Low-temperature mechanochemical synthesis of zinc-substituted hydroxyapatite", *Chem. Sustain. Develop.*, **27** (2019) 251–256.
50. M.V. Chaikina, N.V. Bulina, I.Y. Prosanov, O.B. Vinokurova, A.V. Ishchenko, "Structure formation of zinc-substituted hydroxyapatite during mechanochemical synthesis", *Inorg. Mater.*, **56** (2020) 402–408.
51. S. Keser, A. Dogan, T. Ates, A.A. Barzinjy, B. Ates, S. Tekin, S. Sandal, R.O. Kareem, İ. Özcan, N. Bulut, O. Kaygili, "Effects of gallic acid and quercetin on the structural, thermal, spectroscopic, *in vitro* biocompatibility and electronic properties of Au-based hydroxyapatite structure", *Mater. Chem. Phys.*, **327** (2024) 129892.
52. S. Keser, M. Firat, A.A. Barzinjy, R.O. Kareem, T. Ates, B. Ates, S. Tekin, S. Sandal, İ. Özcan, N. Bulut, O. Kaygili, "Impact of quercetin and gallic acid on the electronic, structural, spectroscopic, thermal properties and *in vitro* bioactivity of silver-modified hydroxyapatite", *Mater. Chem. Phys.*, **339** (2025) 130751.
53. S. Keser, F. Demirbilek, A.A. Barzinjy, R.O. Kareem, B.K. Mahmood, T. Ates, B. Ates, S. Koytepe, N. Bulut, T. İnce, O. Kaygili, "Impact of pyrocatechol on the structural, spectroscopic, thermal characteristics, and *in vitro* bioactivity of gadolinium-enhanced hydroxyapatites", *Inorg. Chem. Comm.*, **178** (2025) 114495.
54. S. Keser, A. Yıldız, A.A. Barzinjy, R.O. Kareem, B.K. Mahmood, R.S. Agid, T. Ates, M.M. Temüz, S. Koytepe, T. İnce, O. Kaygili, J.E. Sienkiewicz, P. Jasik, N. Bulut, "Effects of pyrocatechol on the computational, structural, spectroscopic and thermal properties of silver-modified hydroxyapatite", *J. Aust. Ceram. Soc.*, **61** (2025) 1681–1694.
55. S.F. Mansour, S.I. El-Dek, M.K. Ahmed, "Physico-mechanical and morphological features of zirconia substituted hydroxyapatite nano crystals", *Sci. Rep.*, **7** (2017) 43202.
56. M.J. Robles-Águila, J.A. Reyes-Avendaño, M.E. Mendoza, "Structural analysis of metal-doped (Mn, Fe, Co, Ni, Cu, Zn) calcium hydroxyapatite synthetized by a sol-gel microwave-assisted method", *Ceram. Int.*, **43** (2017) 12705–12709.
57. S. Koutsopoulus, "Synthesis and characterization of hydroxyapatite crystals: A review study on the analytical methods", *J. Biomed. Mater. Res.*, **62** (2002) 600–612.
58. E. Park, R.A. Condrate Sr, D. Lee, K. Kociba, P.K. Gallagher, "Characterization of hydroxyapatite: Before and after plasma spraying", *J. Mater. Sci. Mater. Med.*, **13** (2002) 211–218.
59. O. Kaygili, "Synthesis and characterization of Fe-containing biphasic calcium phosphate ceramics", *J. Aust. Ceram. Soc.*, **55** (2019) 381–385.
60. J. Kamieniak, P.J. Kelly, C.E. Banks, A.M. Doyle, "Mechanical, pH and thermal stability of mesoporous hydroxyapatite", *J. Inorg. Organomet. Polym.*, **28** (2018) 84–91.